Supersolid states in a spin system: Phase diagram and collective excitations

Yuta Murakami,[1] Takashi Oka,[2] and Hideo Aoki[1]
[1]*Department of Physics, The University of Tokyo, Hongo, Tokyo 113-0033, Japan*
[2]*Department of Applied Physics, The University of Tokyo, Hongo, Tokyo 113-8656, Japan*
(Received 21 May 2013; revised manuscript received 6 November 2013; published 4 December 2013)

Phases analogous to supersolids can be realized in spin systems. Here we have obtained, using a bond-operator representation, a mean-field theory and a generalized spin-wave theory, the phase diagram of a frustrated dimer-spin-$\frac{1}{2}$ system on a square lattice and study the collective excitation spectra, focusing on the supersolid (SS) state. In the phase diagram on a parameter space of the exchange interaction and magnetic field, we have identified not only the SS phase, but a phase that has no counterpart in the Bose-Hubbard model and this state becomes dominant at the region where the enhancement of SS occurs in the Bose-Hubbard model. We then investigate the excitation spectrum and spin-spin correlation, detectable by neutron-scattering experiments. We obtain an analytic expression for the spin-wave velocity, which agrees with hydrodynamic relations. The intensity of excitation modes in the spin-spin correlation function is calculated and their change in the supersolid and superfluid states is discussed.

DOI: 10.1103/PhysRevB.88.224404 PACS number(s): 75.10.Jm, 75.40.Gb, 64.70.Tg, 03.75.Kk

I. INTRODUCTION

A supersolid (SS) state is a phase where both off-diagonal long-range order and diagonal long-range order coexist. After the nonclassical rotational inertia experiment in He^4 suggested an SS phase, the SS state attracted considerable interest.[1] However, the interpretation of the result is still controversial,[2] and efforts to find SS continue. Lattice systems are other candidates to find SS than He^4. Cold atoms on optical lattices are one of them. It is suggested that the extended Bose-Hubbard model with a nearest-neighbor interaction shows SS,[3,4] and a technique to realize it is proposed.[5] Dipole-dipole interaction is also suggested to help realize SS.[6,7]

Another, entirely different way to find SS in lattice systems is to consider quantum magnets. This is because certain spin systems can be effectively regarded as Bose systems.[8–10] After a theoretical proposal of SS in a dimer-spin system,[11] spin systems are attracting much attention as a promising candidate to find SS phases.[11–18] One example is the spin-1 Heisenberg model with an anisotropy.[12]

Another example is the spin-$\frac{1}{2}$ dimer model with large Ising-like exchange anisotropy.[11,13,15] While the strong anisotropy in these models are rather unrealistic, it is argued that the model can be effectively realized in a lattice with frustration without anisotropy. With this motivation, Refs. 16 and 17 have investigated a frustrated spin-$\frac{1}{2}$ spin-dimer Heisenberg model with spin-isotropic couplings on a square lattice (Fig. 1) and have shown that the model actually exhibits a SS state. However, these papers are restricted to a specific choice of parameters,[16] or to a study of an effective model from the dimer-spin model.[17] Therefore, the phase diagram in a wider parameter range has not yet been clarified, which should be important for exploring a SS state in real magnets. Further, dynamical properties are also important in examining SS. For instance, in Ref. 19 studying ^{4}He, it has been pointed out that observation of an upper excitation branch by neutron-scattering experiments can be used for searching SS. However, experimentally relevant properties of the SS phase have not been fully understood, and it is important to reveal the excitation spectrum and observability of them with neutron-scattering experiments.

These have motivated us, in the present work, to investigate the phase diagram and dynamical properties of the frustrated spin-$\frac{1}{2}$ dimer Heisenberg model on square lattice. Here, we employ the bond-operator formalism, a mean-field theory, and the generalized spin-wave theory. In the phase diagram on a parameter space of the exchange interaction and the external magnetic field, we have found, on top of the SS phase, a phase that has no counterpart in the Bose-Hubbard model. As for dynamical properties, we study the excitation spectrum and how they can be observed in dynamical spin-spin correlations with inelastic neutron-scattering experiments. We have revealed the behavior of the dynamical properties in the SS and SF phases, especially around their phase boundaries, which can be used as a probe to detect the phase transition experimentally. We have also obtained an analytic expression for the spin-wave velocity, which agrees with hydrodynamic relations. Since the present model has an analogy in cold atoms on optical lattices, our results also give insights into SS in them. For example, one of the correlation functions studied here can be regarded as the dynamical structure factor, which can be detected with Bragg spectroscopy in cold-atom systems.[20,21]

This paper is organized as follows. In Sec. II, we introduce the frustrated spin-$\frac{1}{2}$ dimer Heisenberg model and the bond-operator formalism. We also define the variational wave function for deciding the phase diagram of this model and explain the correspondence to the extended Bose-Hubbard model. Section III is devoted to the phase diagram in the present model in a wide range of parameters. Section IV describes the excitation spectrum and the property of dynamical spin-spin correlations, where we introduce a generalized spin-wave theory. Section V summarizes the paper.

II. FORMALISM

The Hamiltonian of the frustrated spin-$\frac{1}{2}$ dimer Heisenberg model (Fig. 1) is

$$\mathcal{H} = J_0 \sum_i \boldsymbol{S}_{1i} \cdot \boldsymbol{S}_{2i} + J_1 \sum_{\langle i,j \rangle} \boldsymbol{S}_i \cdot \boldsymbol{S}_j + J_2 \sum_{\langle m,i,j \rangle} \boldsymbol{S}_{mi} \cdot \boldsymbol{S}_{mj} - g\mu_B H \sum_i S_i^z, \quad (1)$$

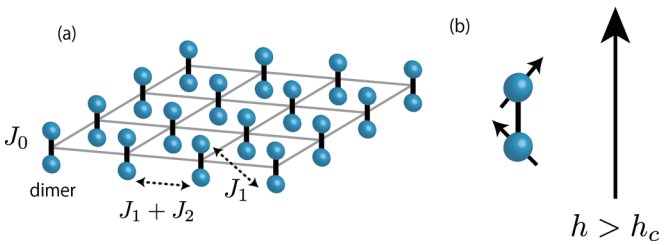

FIG. 1. (Color online) (a) The frustrated spin-$\frac{1}{2}$ dimer Heisenberg model considered here. (b) Spin configuration in a dimer is schematically shown when the magnon BEC occurs for $h \equiv g\mu_B H$ exceeding a critical value(h_c).

where i,j label the dimer's central position, $m = 1,2$ labels the sites within each dimer, and $\boldsymbol{S}_i \equiv \boldsymbol{S}_{1i} + \boldsymbol{S}_{2i}$. Antiferromagnetic exchange interactions comprise intradimer (J_0) and interdimer (J_1, J_2) interactions with $J_0, J_1, J_2 > 0$. Frustration is caused by the J_1 coupling between inequivalent sites between adjacent dimers. Hereafter, we take $J_0 = 1$ as a unit of energy. In the Zeeman energy term, g is the g factor, μ_B the Bohr magneton, and H the external magnetic field.

For treating the spin system, we can adopt the bond-operator formalism,[22–24] in which the four spin states (one singlet and three triplet) in a dimer are described by four bosonic operators, s and t, as

$$\begin{aligned} t_+^\dagger|\mathrm{vac}\rangle &= -|1,1\rangle, \quad s^\dagger|\mathrm{vac}\rangle = |0,0\rangle, \\ t_0^\dagger|\mathrm{vac}\rangle &= |1,0\rangle, \quad t_-^\dagger|\mathrm{vac}\rangle = |1,-1\rangle. \end{aligned} \tag{2}$$

Here $|0,0\rangle$ and $|1,\alpha\rangle$ ($\alpha = \pm,0$) stand for singlet and triplet states, respectively, while $|\mathrm{vac}\rangle$ denotes the vacuum of s,t.

We then only consider the states that satisfy a constraint, $s^\dagger s + \sum_{\alpha=\pm,0} t_\alpha^\dagger t_\alpha = 1$. We note that the bond-operator formalism itself is equivalent to the original expression with spin operators. We opt for this formalism, since this facilitates to identify a correspondence to the extended Bose-Hubbard model, and also enables us to apply a generalized spin-wave theory.

With the bond operators, the Hamiltonian (1) is expressed as

$$\begin{aligned} H = &-\frac{3}{4}J_0\sum_i s_i^\dagger s_i + \left(\frac{J_0}{4} - h\right)\sum_i t_{+i}^\dagger t_{+i} \\ &+ \frac{J_0}{4}\sum_i t_{0i}^\dagger t_{0i} + \left(\frac{J_0}{4} + h\right)\sum_i t_{-i}^\dagger t_{-i} \\ &+ J_2/2\sum_{\langle i,j\rangle} H_{st}(i,j) + (J_1 + J_2/2)\sum_{\langle i,j\rangle} H_{tt}(i,j). \end{aligned} \tag{3}$$

Here $h \equiv g\mu_B H$, and

$$H_{st}(i,j) = \sum_{\alpha=\pm,0}(t_{i\alpha}^\dagger t_{j\alpha} s_j^\dagger s_i + t_{i\alpha}^\dagger t_{j\bar{\alpha}}^\dagger s_j s_i + \mathrm{H.c.}), \tag{4}$$

$$\begin{aligned} H_{tt}(i,j) = &[t_{j0}^\dagger t_{i0}(t_{i+}^\dagger t_{j+} + t_{i-}^\dagger t_{j-}) + \mathrm{H.c.}] \\ &-[t_{i0}t_{j0}(t_{i+}^\dagger t_{j-}^\dagger + t_{i-}^\dagger t_{j+}^\dagger) + \mathrm{H.c.}] \\ &+(t_{i+}^\dagger t_{i+} - t_{i-}^\dagger t_{i-})(t_{j+}^\dagger t_{j+} - t_{j-}^\dagger t_{j-}), \end{aligned} \tag{5}$$

where $\bar{\alpha} = \mp,0$ for $\alpha = \pm,0$, respectively. Using this expression, we can obtain a variational ground-state wave function,

$$\begin{aligned} |\mathrm{GS}\rangle = &\prod_{i\in A}\left(y_A s_i^\dagger + \sum_\alpha x_{A\alpha} t_{i\alpha}^\dagger\right) \\ &\times \prod_{i\in B}\left(y_B s_i^\dagger + \sum_\alpha x_{B\alpha} t_{i\alpha}^\dagger\right)|\mathrm{vac}\rangle, \end{aligned} \tag{6}$$

where the coefficients x, y are complex in general and determined numerically. Here we have divided the square lattice into checkerboard sublattices (A and B), and since the difference between sublattices is allowed, this wave function is capable of describing a SS state. We note that this is nothing but a one-site (dimer) mean-field approximation, which is known to reproduce QMC results semiquantitatively in an anisotropic spin-dimer system.[11] We also see that this approach qualitatively reproduces the results of previous works.[16,17]

A correspondence to Bose systems can be seen when the ground state does not involve the $|1,0\rangle$ state ($x_0 = 0$).[23] We have numerically confirmed that this situation is, in fact, realized in most parts of the phase diagram. In this case, the Hamiltonian excluding $|1,0\rangle$ from the beginning gives the same ground state, and the Hamiltonian reduces to

$$\begin{aligned} H_{\mathrm{eff}} = &\frac{J_2}{2}\sum_{\langle i,j\rangle}[(t_{i+}^\dagger s_i + s_i^\dagger t_{i-})(s_j^\dagger t_{j+} + t_{j-}^\dagger s_j) + \mathrm{H.c.}] \\ &+\left(J_1 + \frac{J_2}{2}\right)\sum_{\langle i,j\rangle}(t_{i+}^\dagger t_{i+} - t_{i-}^\dagger t_{i-})(t_{j+}^\dagger t_{j+} - t_{j-}^\dagger t_{j-}) \\ &+ J_0\sum_i(t_{i+}^\dagger t_{i+} + t_{i-}^\dagger t_{i-}) - h\sum_i(t_{i+}^\dagger t_{i+} - t_{i-}^\dagger t_{i-}), \end{aligned} \tag{7}$$

with a constraint $s_i^\dagger s_i + \sum_{\alpha=\pm} t_{i\alpha}^\dagger t_{i\alpha} = 1$. We note that this coincides with the anisotropic spin-1 Heisenberg model used in Ref. 12.

We can effectively identify this model with an extended Bose-Hubbard model,

$$\begin{aligned} H = &-t\sum_{\langle i,j\rangle}(a_i^\dagger a_j + \mathrm{H.c.}) - \mu\sum_i n_i \\ &+ V\sum_{\langle i,j\rangle} n_i n_j + U\sum_i n_i n_i, \end{aligned} \tag{8}$$

where $a^\dagger$ is the boson creation operator, $\langle i,j\rangle$ the nearest neighbors, μ the boson chemical potential, U the on-site Hubbard interaction, and V the nearest-neighbor interaction. To do this, we truncate the states to three states up to the doubly occupied state in the extended Hubbard model, identify $t_-^\dagger|\mathrm{vac}\rangle = |0\rangle$, $s^\dagger|\mathrm{vac}\rangle = |1\rangle$, $t_+^\dagger|\mathrm{vac}\rangle = |2\rangle$, and express Eq. (8) in terms of t, s as in Ref. 20. This procedure is known as the Schwinger-Boson approach. Then it turns out that the spin model Eq. (7) can be regarded as the extended Hubbard model through

$$\begin{aligned} J_2/2 \leftrightarrow -t, \quad J_1 + J_2/2 \leftrightarrow V, \\ J_0 \leftrightarrow U/2, \quad h \leftrightarrow \delta\mu, \end{aligned} \tag{9}$$

where $\delta\mu \equiv \mu - \frac{U}{2} - ZV$, with Z being the coordination number. Strictly speaking, there is only slight difference in the

TABLE I. Correspondence between the dimer-spin system and the Bose system. In the Bose system, $|n\rangle$ represents a state with n bosons, and n_A,n_B is the boson density on A, B sublattices, respectively. For the spin system the bond-operator representation is used.

Spin-$\frac{1}{2}$ dimer system	Bose system
States: $t_-^\dagger|\text{vac}\rangle$, $s^\dagger|\text{vac}\rangle$, $t_+^\dagger|\text{vac}\rangle$	States: $|0\rangle$,$|1\rangle$,$|2\rangle$
In-plane magnetization: $M_{xy} = \langle S_1^+ - S_2^+\rangle/\sqrt{2}$	Order parameter: $\langle a^\dagger\rangle$
In-plane staggered magnetization:	Condensate density:
$n_c = (\frac{1}{N}\sum_i \langle S_{i,1}^+ - S_{i,2}^+\rangle e^{i\boldsymbol{Q}\cdot\boldsymbol{r}_i}/\sqrt{2})^2$	$n_c = \|\frac{1}{N}\sum_i \langle a_i^\dagger\rangle\|^2$
Staggered magnetization:	Staggered occupation number:
$m_z^{\text{st}} = \frac{1}{2N}\sum_i \langle S_{i,1}^z + S_{i,2}^z\rangle e^{i\boldsymbol{Q}\cdot\boldsymbol{r}_i}$	$n^{\text{st}} = (n_A - n_B)/2$
Averaged magnetization: $m_z = \frac{1}{2N}\sum_i \langle S_{i,1}^z + S_{i,2}^z\rangle$	Averaged occupation number: $n = (n_A + n_B)/2$

hopping terms. In the truncated Hubbard model it is written as $-t\sum_{\langle i,j\rangle}[(\sqrt{2}t_{i+}^\dagger s_i + s_i^\dagger t_{i-})(\sqrt{2}s_j^\dagger t_{j+} + t_{j-}^\dagger s_j) + \text{H.c.}]$, where $\sqrt{2}t_{i+}^\dagger s_i + s_i^\dagger t_{i-}$ corresponds to the creation operator $a^\dagger$ in the truncated space. On the other hand, in the case of the spin model, we regard $t_{i+}^\dagger s_i + s_i^\dagger t_{i-}$ as the creation of a boson; see Eq. (7).[23]

Thus, the spin-$\frac{1}{2}$ model is effectively a *semi-hard-core boson system* in regions in the phase diagram where the $|1,0\rangle$ state can be ignored.[23] In order to compare the phase diagrams of the two systems, it is useful to draw the phase diagrams with the parameter corresponding to V fixed, since phase diagrams of the extended Bose-Hubbard model is often written in this way.

From the above correspondence, we can naturally define the order parameters: The in-plane magnetization $M_{xy,i} = \langle S_{i,1}^+ - S_{i,2}^+\rangle/\sqrt{2}$, which denotes the difference of the magnetization in the spins in each dimer, represents the breakdown of the U(1) symmetry in the spin model, which corresponds to $\langle a^\dagger\rangle$ in the Bose-Hubbard model with a broken U(1) symmetry (the order parameter in BEC). Thus, the averaged condensate density is $n_c = (\frac{1}{N}\sum_i \langle S_{i,1}^+ - S_{i,2}^+\rangle e^{i\boldsymbol{Q}\cdot\boldsymbol{r}_i}/\sqrt{2})^2$, where $\boldsymbol{Q} = (\pi,\pi)$ and N the total number of sites. Note that the factor $e^{i\boldsymbol{Q}\cdot\boldsymbol{r}_i}$ takes care of the fact that $J_2 > 0$ induces antiferroic ordering. In the terminology of the Bose-Hubbard model, this is because the hopping term is positive; see Eq. (9). The z-component staggered magnetization, $m_z^{\text{st}} = \frac{1}{2N}\sum_i \langle S_{i,1}^z + S_{i,2}^z\rangle e^{i\boldsymbol{Q}\cdot\boldsymbol{r}_i}$, represents the breaking of the Z_2 symmetry (the symmetry between A,B sublattices). Another important quantity is the uniform magnetization $m_z = \frac{1}{2N}\sum_i \langle S_{i,1}^z + S_{i,2}^z\rangle$, which corresponds to the density of bosons in the Hubbard model. The correspondence is summarized in Table I.

III. PHASE DIAGRAM

Figure 2 shows the phase diagram against h and J_2 obtained by optimizing the variational wave function Eq. (6). The plot is a counterpart in the spin system of a phase diagram for the

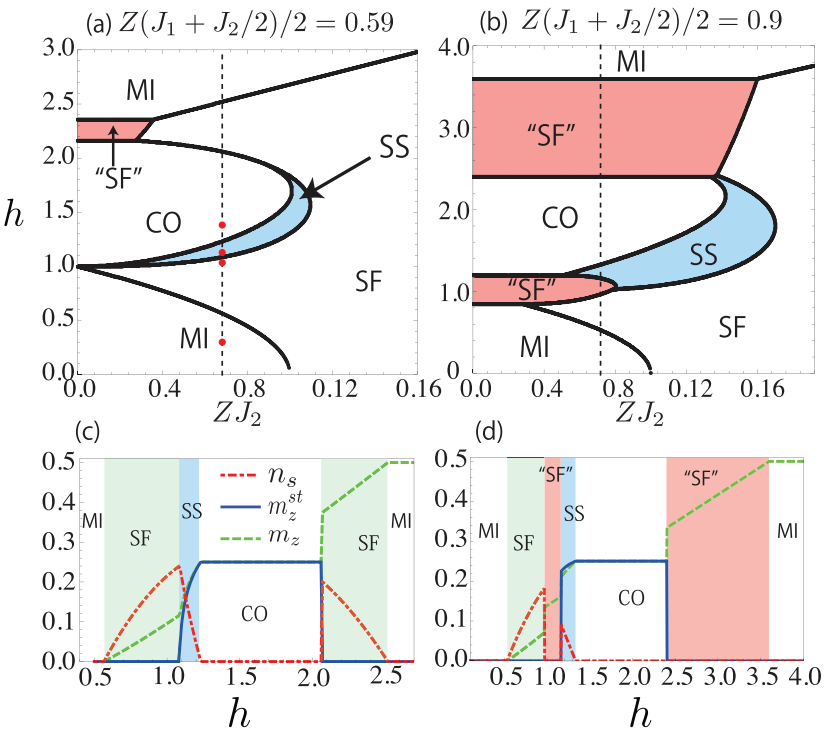

FIG. 2. (Color online) Ground-state phase diagram for $Z(J_1 + J_2/2)/2 = 0.59$ (a) and 0.9 (b), with Z being the coordination number [i.e., $ZV = 0.59U$ (a), $ZV = 0.9U$ (b) for the boson model]. The parameters h and ZJ_2 correspond to the chemical potential $\delta\mu$ and hopping parameter $-t$, respectively, in the boson system. Phases are denoted by SS (supersolid), SF (superfluid), MI (Mott insulator), and CO (charge-ordered phase), while "SF" stands for a phase that has no counterpart in the Bose system. Various order parameters are plotted against h in (c) for $Z(J_1 + J_2/2)/2 = 0.59$, $ZJ_2 = 0.68$, and in (d) for $Z(J_1 + J_2/2)/2 = 0.9$, $ZJ_2 = 0.72$. The dashed lines in (a),(b) indicate the cross sections at which (c),(d) are plotted, respectively. Red dots in (a) indicate the points at which the excitation spectra are displayed in Fig. 3 below.

TABLE II. Correspondence of phases between the dimer-spin system and the Bose system. n is the averaged occupation number of boson.

Spin-$\frac{1}{2}$ dimer system	Bose system
$n_c = 0, m_z^{\rm st} = 0,$	Mott-insulating phase (MI)
$m_z = 0.0$	for $n = 1$
$n_c = 0, m_z^{\rm st} = 0$	Mott-insulating phase (MI)
$m_z = 0.5$	for $n = 2$
$n_c \neq 0, m_z^{\rm st} = 0$	Superfluid (SF)
$n_c = 0, m_z^{st} \neq 0$	Charge-ordered state (CO)
$n_c \neq 0, m_z^{\rm st} \neq 0$	Supersolid (SS)

Bose-Hubbard model against the chemical potential ($\delta\mu$) and hopping parameter ($-t$). The two panels [(a),(b)] correspond to different values of ZV, which is the effective nearest-neighbor interaction $V = J_1 + J_2/2$ multiplied by the coordination number Z. Thus, panels (a) and (b) for $Z(J_1 + J_2/2)/2 = 0.59$ and 0.9 correspond to those for the Bose system at $ZV = 0.59U$ and $0.9U$, respectively. To specify the phases, here we adopt the terminology from the Bose-Hubbard model, see Table II. In particular, superfluid (SF) is a phase with $n_c \neq 0$ and $m_z^{\rm st} = 0$, while a SS state is a phase with $n_c \neq 0$ and $m_z^{\rm st} \neq 0$ simultaneously.

First, the SS phase in the present spin model appears adjacent to, and mainly in the lower half of, the CO phase. We note that this feature is also seen in the phase diagram of the extended Bose-Hubbard model.[4] At the boundary of MI the excitation gap closes, and the boundary can be given analytically, where the lower density branch is $h = \sqrt{1 - ZJ_2}$, while the higher one is $1 + ZJ_1 + ZJ_2$, within our approximation. Figure 2(c) shows the h dependence [on a cross section indicated in (a)] of relevant order parameters for $ZJ_1 = 0.84$ and $ZJ_2 = 0.68$. As can be seen, within the mean-field analysis, the transition between MI/SF, SF/SS, and SS/CO are of second order, while that between SF/CO is of first order. It turns out that the results agree qualitatively well with those obtained with the infinite time-evolving block decimation (iTEBD) combined with the tensor renormalization group (TRG) approach[16] and the self-consistent cluster mean-field analysis of an effective model.[17] This supports the validity of our method for this model.

Curiously, we find regions where we cannot neglect the existence of $t_0^\dagger$, which we call "SF", while in other regions we can. This phase has not been recognized in the previous works on this model.[16,17] In the "SF" regions [red regions in Figs. 2(a) and 2(b)], the coefficient of $s^\dagger$ in Eq. (6) vanishes. The wave function takes a form,

$$|\mathrm{GS}\rangle = \prod_{i\in A}(x_+ t_{i+}^\dagger + x_0 t_{i0}^\dagger + x_- t_{i-}^\dagger) \times \prod_{i\in B}(-x_+ t_{i+}^\dagger + x_0 t_{i0}^\dagger - x_- t_{i-}^\dagger)|\mathrm{vac}\rangle, \quad (10)$$

where x_α's are real. Note that this state breaks a U(1) symmetry (i.e., the symmetry around Z axis). The character of this state becomes clearer when we project the original Hamiltonian [Eq. (1)] into the space consisting only of triplets on each dimer to have

$$H' = (J_1 + J_2/2)\sum_{\langle i,j\rangle} \boldsymbol{S}'_i \cdot \boldsymbol{S}'_j + h\sum_i S_i'^z, \quad (11)$$

which is nothing but the simplest isotropic spin-1 Heisenberg model in an external magnetic field h. Here $\boldsymbol{S}'$ denotes the spin-1 spin operator, e.g., $S'^z = t_+^\dagger t_+ - t_-^\dagger t_-$ in bond operators. Then we can regard the "SF" state as a *canted antiferromagnet* in the Heisenberg model. Comparing Figs. 2(a) and 2(b), we notice that the SS region becomes wider as the repulsion V becomes stronger. The "SF" region also expands, where SS and "SF" phases compete with each other. Figure 2(d) plots relevant order parameters against h [on a cross section indicated in (b)] for $ZJ_1 = 1.44$ and $ZJ_2 = 0.72$. For this set of parameters, phase transitions occur six times as the external field is increased. Specifically, the transition from SF to "SF" is seen to be discontinuous.

Let us compare the present result with that for the extended Bose-Hubbard model. In the latter, the SS region becomes wider when the nearest-neighbor repulsion V is increased. Moreover, when $ZV > U$, there is no MI and all insulating phases are CO, while the SS region becomes even wider.[25] These behaviors are contrasted with the present phase diagram for the spin model for $ZV > U$, where, contrary to a naive expectation, it turns out that SS does not expand, but gives way to "SF" for a fixed V, and that the SS region is completely suppressed by "SF" for large-enough V (not shown). Thus, we do have differences between the spin and the Bose models. To sum up, our analysis indicates that competition between SS and "SF" phases should be taken into account in examining SS in this system, besides the instability for domain wall formation discussed in Ref. 17.

IV. DYNAMICAL PROPERTIES

We now reveal dynamical properties such as excitation spectrum and dynamical spin-spin correlations around SS in the magnetic system Eq. (1), which can be regarded as an effective semi-hard-core Bose system. To this end, we employ a generalized spin-wave theory. The similar type of analysis has been applied to a bilayer Heisenberg model[22] and an anisotropic spin-1 Heisenberg model[26,27] for investigating SF[22,26] and MI[22,26,27] in our terminology. We also note that this type of analysis works well in investigating real materials.[24] We mainly focus on the behavior around SS, which has not been clarified.

A. Excitations

Let us move on to the study of excitation spectra. Here we employ a generalized spin-wave theory which is applicable except for the "SF" phase.[22] We convert the Hamiltonian Eq. (3) into an effective one by introducing boson operators $\{b\}$ with a canonical transformation,

$$\begin{aligned} b_{0i}^\lambda &= u_\lambda s_i + v_\lambda(f_\lambda t_{+i} + g_\lambda t_{-i}), \\ b_{+i}^\lambda &= -v_\lambda s_i + u_\lambda(f_\lambda t_{+i} + g_\lambda t_{i-}), \\ b_{00i}^\lambda &= t_{0i}, \quad b_{-i}^\lambda = -g_\lambda t_{i+} + f_\lambda t_{i-}. \end{aligned} \quad (12)$$

Here $\lambda = \mathrm{A}$ or B and u, v, f, and g (with $u^2 + v^2 = 1$ and $f^2 + g^2 = 1$) are real and defined in such a way that the ground state is $(\prod_{i\in A} b_{0i}^{A\dagger})(\prod_{j\in B} b_{0j}^{B\dagger})|\mathrm{vac}\rangle$. After this transformation, the constraint is converted to $b_{0i}^{\lambda\dagger} b_{0i}^{\lambda} + \sum_{\theta} b_{\theta,i}^{\lambda\dagger} b_{\theta,i}^{\lambda} = 1$, where $\theta = \pm, 00$. Then we deal with the constraint in terms of the Holstein-Primakoff (HP) transformation,

$$b_{0i}^{\lambda} = b_{0i}^{\lambda\dagger} = \left(1 - \sum_{\theta} \hat{n}_{\theta,i}^{\lambda}\right)^{1/2}, \tag{13}$$

where $\hat{n}_{\theta,i}^{\lambda} = b_{\theta,i}^{\lambda\dagger} b_{\theta,i}^{\lambda}$.

If we plug this into the Hamiltonian and neglect the terms with more than two boson operators (which amounts to the linear spin-wave approximation), the effective Hamiltonian takes a form, $H_{\mathrm{eff}} = H_{\mathrm{eff}\pm} + H_{\mathrm{eff}0}$, where $H_{\mathrm{eff}\pm}$ is composed of $b_{\pm}^{\dagger}$ and $H_{\mathrm{eff}0}$ is composed of $b_{00}^{\dagger}$. The form of $H_{\mathrm{eff}\pm}$ is, up to a constant,

$$H_{\mathrm{eff}\pm} = \frac{1}{2} \sum_{\mathbf{k}\in \mathbf{BZ}/2} \boldsymbol{\psi}_{\mathbf{k}}^{\dagger} \hat{H}_{\mathrm{eff}\pm}(\mathbf{k}) \boldsymbol{\psi}_{\mathbf{k}}, \tag{14}$$

where $\boldsymbol{\psi}_{\mathbf{k}} = (b_{\mathbf{k},+}^{A}, b_{\mathbf{k},-}^{A}, b_{\mathbf{k},+}^{B}, b_{\mathbf{k},-}^{B}, b_{-\mathbf{k},+}^{A\dagger}, b_{-\mathbf{k},-}^{A\dagger}, b_{-\mathbf{k},+}^{B\dagger}, b_{-\mathbf{k},-}^{B\dagger})^{T}$, and $\hat{H}_{\mathrm{eff}\pm}$ is an 8×8 matrix, whose components are shown in an appendix. The folded Brillouin zone $\mathbf{BZ}/2$ denotes the first Brillouin zone when the symmetry between A and B sublattices is broken; see Fig. 3(f). We can diagonalize the effective Hamiltonian as

$$H_{\mathrm{eff}\pm} = \sum_{\mathbf{k}\in \mathbf{BZ}/2,\tau} \epsilon_{\tau}(\mathbf{k}) \beta_{\mathbf{k},\tau}^{\dagger} \beta_{\mathbf{k},\tau}, \tag{15}$$

with the band index $\tau = 1$–4. Here we have applied a Bogoliubov transformation U: $\boldsymbol{\psi}'_{\mathbf{k}} = U\boldsymbol{\psi}_{\mathbf{k}}$, where U is an 8×8 matrix satisfying $U\Sigma U^{T} = \Sigma$, with $\Sigma = \mathrm{diag}(1,1,1,1,-1,-1,-1,-1)$ and $\boldsymbol{\psi}'_{\mathbf{k}} = (\beta_{\mathbf{k},1}, \beta_{\mathbf{k},2}, \beta_{\mathbf{k},3}, \beta_{\mathbf{k},4}, \beta_{-\mathbf{k},1}^{\dagger}, \beta_{-\mathbf{k},2}^{\dagger}, \beta_{-\mathbf{k},3}^{\dagger}, \beta_{-\mathbf{k},4}^{\dagger})^{T}$ (Ref. 20). $\beta_{\mathbf{k},\tau}^{\dagger}$ creates a spin wave. The ground state with the spin-wave correction included is the vacuum of spin waves and denoted as $|\phi_0\rangle$ in the following. Note that the above is applicable to SF and MI phases. There, the excitation spectrum appears to have four bands since we treat them in the folded Brillouin zone $\mathbf{BZ}/2$. When we unfold the Brillouin zone into the full **BZ**, it has two bands. Note that the main difference between the results in SS and those in SF within this method is that there are no degenerated modes at the boundary of $\mathbf{BZ}/2$ in SS. We also note that one can evaluate the expectation value of physical quantities in this approximation as follows. An operator representing a quantity is first transformed with b. Then the HP transformation is applied to $b_0^{\lambda}, b_0^{\lambda\dagger}$, and the expansion is made up to the order needed. When $b_0^{\lambda}, b_0^{\lambda\dagger}$ appear in the form of $n_{\lambda 0}$, this can be dealt with using the constraint directly. Finally, we take the expectation value for the transformed operator.

In Figs. 3(a)–3(d), we show the excitation spectrum in the phases MI, SF, SS, and CO, respectively, for which the positions on the phase diagram are indicated in Fig. 2(a). While some of the natures of MI and SF have already been well investigated,[22,26,27] we display the results in order to compare them with the results for SS or CO, and to show a precursor of SS or CO in SF. The spectrum is drawn along the (1,1) direction ($k_x = k_y$). Here we only show the excitations composed of $b_{\pm}$, since only these modes have the counterparts in the Bose-Hubbard model. In MI and SF, there are two excitation bands. On the other hand, in SS and CO, there are four bands because the symmetry between A,B sublattices is broken. There is a gap in MI ($n = 1$), and the two (three if t_0 is included) modes are degenerate at $h = 0$. As h increases, the degeneracy is lifted due to the Zeeman splitting [Fig. 3(a)]. The dispersion relation is given by

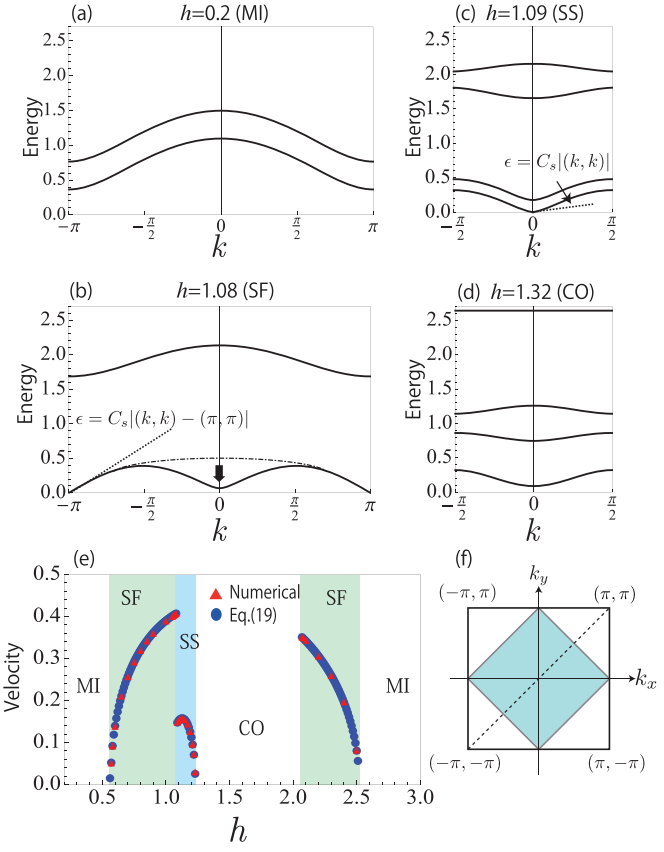

FIG. 3. (Color online) Excitation spectra against $k_x = k_y = k$ for a Mott insulator at $h = 0.2$ (a), SF at $h = 1.08$ (b), SS at $h = 1.09$ (c), and charge order at $h = 1.32$ (d), with $ZJ_1 = 0.84$ and $ZJ_2 = 0.68$. They correspond to four red dots in Fig. 2(a). Dotted lines in (b) and (c) represent the velocity of a NG mode. In (b) a dash-dotted line represents the first excitation band away from the SS/SF boundary, where an arrow indicates how the dispersion dips into the origin. (e) The velocity of Nambu-Goldstone mode against h. Blue dots are derived directly from the excitation spectra, while red dots represent Eq. (19). (f) The original Brillouin zone (**BZ**; large square) for the phases without Z_2 breaking symmetry, and the folded Brillouin zone ($\mathbf{BZ}/2$; blue area) for phases with the broken symmetry are indicated. The dotted line shows the $k_x = k_y = k$ direction.

$$\epsilon(\mathbf{k}) = \sqrt{J_0^2 + 2J_0J_2\gamma(\mathbf{k})} \pm h, \tag{16}$$

where $\gamma(\mathbf{k}) = \sum_{a=1}^{d} \cos(k_a)$ with a labeling the axes.[22,26,27] When the gap closes, a quantum phase transition between SF and MI occurs. In the SF phase, there is one gapless mode [a Nambu-Goldstone (NG) mode; recently, the problem of NG

mode has attracted renewed interest[28,29]], which arises from the U(1) symmetry breaking. In particular, the velocity of the NG mode vanishes along the boundary except at $h = 0, ZJ_2 = J_0$ (Refs. 22 and 26), where the universality class of the phase transition changes from the rest (field induced phase transition to SF). The other band is a massive mode. As h becomes closer to the SF/SS boundary, a dip (i.e., softening) appears in the mode around $\mathbf{k} = (0,0)$, and we observe that the gap closes at the boundary [Fig. 3(b)]. This mode can be thought of as a *roton mode*, which represents a softening into CO or SS. Note that the roton is located at the zone center rather than a zone boundary, since the hopping parameter is positive in our model. If we turn to the excitation spectrum of SS state in Fig. 3(c), there is one NG mode with a linear dispersion. The roton mode in SF near SS and the NG mode with a linear dispersion have been observed in SS in hard-core boson systems[30,31] or in an extended Bose-Hubbard model (a soft-core system).[3] Here we have revealed that the semi-hard-core Bose system also shares these behaviors. At the boundary of SS and CO, the velocity of the NG mode becomes 0. In the CO phase, there is an energy gap, which is closed at the boundary between CO and SS, and the highest mode is flat with $\epsilon(\mathbf{k}) = 2h$ [Fig. 3(d)]. In this mode up-spin triplet flips into a down-spin triplet. The rest of the excitation spectrum can be obtained by solving an equation cubic in x for each $\mathbf{k}$,

$$0 = [x + h - J_0 - Z(J_1 + J_2/2)](x + h - J_0) \times [x + h + J_0 - Z(J_1 + J_2/2)] + 2J_0J_2^2\gamma(\mathbf{k})^2. \quad (17)$$

Strictly speaking, the actual excitation corresponds to the absolute value of the solution. From the structure of the equation and straightforward manipulation, we notice that the dispersion does not change against h, and the energy of one of the bands decreases as h increases. Therefore, there occurs a band crossing at some h in CO. In addition, one can show analytically that a band never has linear dispersion at the point where the gap in CO spectrum is closed. This contrasts with the case of MI ($n = 1$), where, at $h = 0$ and $ZJ_2 = J_0$, the gap is closed but the band has a linear dispersion; see Eq. (16). It is numerically confirmed that, at the SF/CO boundary, the gap in the CO phase does not close, nor does the roton mode. (Near the CO/SF boundary, a roton mode appears again.) The velocity of the NG mode approaches zero toward the boundary of SF and MI ($n = 2$). In the latter phase, the upper band is flat [$\epsilon(\mathbf{k}) = 2h - 2Z(J_1 + J_2/2)$]. The analytic expression[26] for the other band is

$$\epsilon(\mathbf{k}) = -J_0 + h - Z\left(J_1 + \frac{J_2}{2}\right) + J_2\gamma(\mathbf{k}). \quad (18)$$

To gain further understanding of the excitations, we show an analytic expression for the spin-wave velocity (with the derivation given in an Appendix),

$$C_s = \left(\frac{J_2}{2\kappa}|M_{xy,A}M_{xy,B}|\right)^{1/2}, \quad (19)$$

where $\kappa = \partial m_z/\partial h$ denotes the spin susceptibility, and $M_{xy,A}, M_{xy,B}$ the magnetization of each sublattice. Note that M_{xy} and m_z here do not include spin-wave corrections, though it is not negligible in two dimensions. This microscopic expression is consistent with the relation derived from phenomenological discussions (hydrostatically or with an effective Lagrangian) for spin systems[32] and for Bose systems,[33,34] which is $C_s^2 = \rho_s/\chi$. Here ρ_s is the spin stiffness or the SF density and χ is the spin susceptibility or the compressibility. This relation has been expected to be satisfied in this method, where the consistency has been pointed out in Ref. 22. What we have done here is to concretely derive the analytic expression for C_s in the generalized spin-wave method including SS. We also note that the Gutzwiller approximation for the Bose-Hubbard model gives a similar expression for SF (Ref. 21). We can also show that the above expression holds in SS when the Gutzwiller approximation is used for the extended Bose-Hubbard model. The velocity plotted against h from Eq. (19) is displayed in Fig. 3(e) along with the numerical result, and we can see that the two sets of results exactly coincide with each other. Then, a jump in the velocity at the SF/SS boundary can be attributed to a jump in the spin susceptibility. The velocity vanishes at MI/SF and SS/CO boundaries, since M_{xy} becomes 0.

Next, we discuss the properties of collective excitation modes. We focus on all four modes for small $\mathbf{k}$ along the (1,1) direction in the folded Brillouin zone $\mathbf{BZ}/2$. (For SF, a NG mode, a roton mode, a massive mode and the rest are investigated.) To reveal the character of each excitation ($\beta^\dagger_{\mathbf{k},\tau}$), we construct a coherent state ($|\chi_{\mathbf{k},\tau}\rangle$) to calculate the spatial variation of $m_{z,i}$ ($=\langle S^z_{i,1} + S^z_{i,2}\rangle$) and $M_{xy,i}$. In the boson language the former corresponds to spatial density modulations, while the latter corresponds to modulations of the order parameter ($\langle a^\dagger\rangle$). The coherent state is expressed as

$$|\chi_{\mathbf{k},\tau}\rangle = \exp(-|\chi_{\mathbf{k},\tau}|^2/2)\exp(\chi_{\mathbf{k},\tau}\beta^\dagger_{\mathbf{k},\tau})|\phi_0\rangle. \quad (20)$$

Here we choose $\chi_{\mathbf{k},\tau}$ to be small, which amounts to assuming that there are not too many spin waves. In SF, it turns out that, except for the third excitation mode [a massive mode in Fig. 3(b) near $k \approx \pi$], excitation modes are accompanied by both a modulation of the order parameter (i.e., condensate density) and the density. On the other hand, the massive mode does not exhibit modulation in the density but shows a local imbalance between condensate and noncodensate amplitudes, as seen in Fig. 4(a). This agrees with the result for cold atoms.[20] In the SS phase, by contrast, such a mode disappears, as seen in Fig. 4(b). All the four modes in SS are accompanied by modulations of density and order parameter. Figures 4(c) and 4(d) display the spatial variation of the phase [$\mathrm{Arg}(M_{xy})$] of $M_{xy,A}$, $-M_{xy,B}$ ($\equiv\Delta\theta$) for the second excitation mode (the roton mode) at $h = 1.08$ (SF) and $h = 1.09$ (SS), respectively. Note that the minus sign in $-M_{xy,B}$ again comes from the antiferromagneic coupling J_2. We can see that the relation of the phase modulation between A and B sublattice is different between SF and SS. In SF, the roton mode may be thought of as a Leggett mode if we regard one cell as composed of two neighboring sites (one belongs to A sublattice, and the other to B), since the phase of the order parameter out phase between A and B sublattices. On the other hand, this interpretation cannot be applied to SS, where the phase modulation is in phase between them. We have to note that this property of the second excitation in the SS phase changes for large enough V and away form the SS/SF boundary. Then the phase modulation

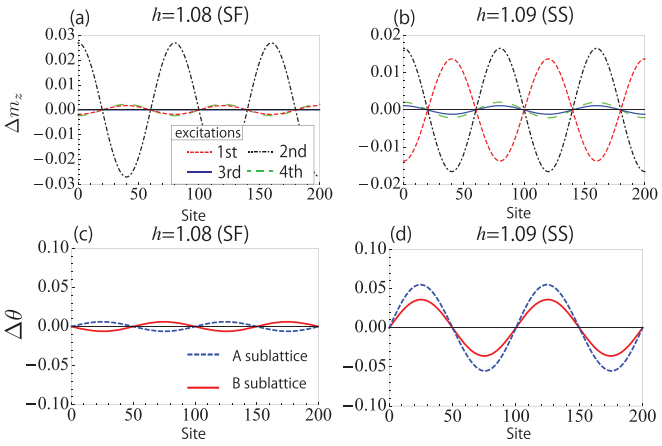

FIG. 4. (Color online) Spatial variation of physical quantities for excitation modes for small k in $\mathbf{BZ}/2$. We have chosen parameters $ZJ_1 = 0.84$ and $ZJ_2 = 0.68$. Panels (a) and (b) show the modulation of the density from the equilibrium value (Δm_z) in A sublattice at $h = 1.08$ (SF) and $h = 1.09$ (SS), respectively. The red line represents the first excited mode (a NG mode), the black line the second excitation (roton) mode, the blue line the third excitation (massive) mode, and the green line the fourth mode. Panels (c) and (d) show the spatial variation of the phase of $M_{xy,A}$ and $-M_{xy,B}$ for the second excitation mode for $h = 1.08$ (c) or $h = 1.09$ (d).

becomes out of phase between A and B sublattices (as in SF). As for the NG mode, the spatial modulation of the phase of the order parameter (not shown) is in phase between A and B sublattices in both of the states.

B. Spin-spin correlation

Analysis of spin-spin correlations is important from the experimental viewpoint, since inelastic neutron scattering can detect it. Here we focus on two kinds of spin-spin correlations that have counterparts in Bose systems. The first one is

$$C^z(\mathbf{k},\omega) \equiv \int_{-\infty}^{\infty} d\tau e^{i\omega\tau} \left\langle S^z_{\mathbf{k}}(\tau) S^z_{-\mathbf{k}}(0) \right\rangle = \sum_n \left| \langle n|S^z_{-\mathbf{k}}|\phi_0\rangle \right|^2 \delta(\omega - \epsilon_n), \tag{21}$$

where $S^z_i \equiv S^z_{1,i} + S^z_{2,i} = t^\dagger_+ t_+ - t^\dagger_- t_-$, $|\phi_0\rangle$ denotes the ground state and $|n\rangle$ denotes an excited state with an energy ϵ_n. The correlation function corresponds to the dynamical structure factor in cold-atom systems, which can be detected with Bragg spectroscopy and which has been theoretically investigated in this context.[20,21] The second correlation function is

$$C^{+-}(\mathbf{k},\omega) \equiv \int_{-\infty}^{\infty} d\tau e^{i\omega\tau} \langle \hat{M}_{xy,-\mathbf{k}}(\tau) \hat{M}^\dagger_{xy,-\mathbf{k}}(0) \rangle = \sum_n |\langle n|\hat{M}^\dagger_{xy,-\mathbf{k}}|\phi_0\rangle|^2 \delta(\omega - \epsilon_n). \tag{22}$$

Here $\hat{M}_{xy,i} \equiv (S^+_{1,i} - S^+_{2,i})/\sqrt{2} = t^\dagger_{+i} s_i + s^\dagger_i t_{i-}$, which is an operator form of $M_{xy,i}$ introduced before. This correlation function corresponds to the lesser Green's function $G^<_{-\mathbf{k}}(\omega) \equiv -i \int_{-\infty}^{\infty} d\tau e^{i\omega\tau} \langle a^\dagger_{-\mathbf{k}}(\tau) a_{-\mathbf{k}}(0) \rangle$, where a is a bosonic annihilation operator. We note that, with in the linear spin-wave theorem, these correlations do not have contribution from the spin wave consisting of $t_0, t^\dagger_0$. There are n-spin wave states defined as $(\beta^\dagger)^n|\text{vac}\rangle$ in the spin-wave theory. In the following, we focus on the intensity of the single spin-wave peak by taking $|\mathbf{k},\tau\rangle = \beta^\dagger_{\mathbf{k},\tau}|\text{vac}\rangle$ as $|n\rangle$, where $\beta^\dagger_{\mathbf{k},\tau}$ is defined in Eq. (15). Within the spin-wave theory, one can evaluate the coefficient of the δ function [$\delta(\omega - \epsilon_n)$ in Eqs. (21) and (22)] as

$$\begin{aligned} &\langle \tau, -\mathbf{k}_0|S^z_{-\mathbf{k}}|\phi_0\rangle \\ &= \sqrt{\frac{N}{2}} \sum_\lambda \left\{ v_\lambda u_\lambda \left(f^2_\lambda - g^2_\lambda\right) e^{i\mathbf{G}\cdot\mathbf{l}_\lambda} [N_{(\lambda,+)\tau}(\mathbf{k}_0) + P_{(\lambda,+)\tau}(\mathbf{k}_0)] \right. \\ &\quad \left. - 2v_\lambda g_\lambda f_\lambda e^{i\mathbf{G}\cdot\mathbf{l}_\lambda} [N_{(\lambda,-)\tau}(\mathbf{k}_0) + P_{(\lambda,-)\tau}(\mathbf{k}_0)] \right\} \end{aligned} \tag{23}$$

and

$$\begin{aligned} &\langle \tau, -\mathbf{k}_0|\hat{M}^\dagger_{xy,-\mathbf{k}}|\phi_0\rangle \\ &= \sqrt{\frac{N}{2}} \sum_\lambda e^{i\mathbf{G}\cdot\mathbf{l}_\lambda} \left[\left(u^2_\lambda g_\lambda - v^2_\lambda f_\lambda\right) N_{(\lambda,+),\tau}(\mathbf{k}_0) \right. \\ &\quad + \left(u^2_\lambda f_\lambda - v^2_\lambda g_\lambda\right) P_{(\lambda,+),\tau}(\mathbf{k}_0) + u_\lambda f_\lambda N_{(\lambda,-),\tau}(\mathbf{k}_0) \\ &\quad \left. - u_\lambda g_\lambda P_{(\lambda,-),\tau}(\mathbf{k}_0) \right], \end{aligned} \tag{24}$$

where $\mathbf{l}_\lambda$ is an arbitrary site in the sublattice λ, $\mathbf{G}$ is $(\pm\pi, \pm\pi)$ or $(0,0)$ chosen so that $\mathbf{k}_0$ be in $\mathbf{BZ}/2$, and $\mathbf{k} = \mathbf{k}_0 + \mathbf{G}$. $P(\mathbf{k})$ and $N(\mathbf{k})$ are the elements of the matrix used for the Bogoliubov transformation [Eq. (15)],

$$U(\mathbf{k}) = \begin{pmatrix} N(\mathbf{k}) & P(\mathbf{k}) \\ P(\mathbf{k}) & N(\mathbf{k}) \end{pmatrix}, \tag{25}$$

where the elements of 4×4 N, P are denoted as $N_{(\lambda,\theta),\tau}, P_{(\lambda,\theta),\tau}$. The intensity of a single spin-wave mode is expressed as $|\langle \tau, -\mathbf{k}_0|S^z_{-\mathbf{k}}|\phi_0\rangle|^2$ for $C^z(\mathbf{k},\omega)$ and $|\langle \tau, -\mathbf{k}_0|\hat{M}^\dagger_{xy,-\mathbf{k}}|\phi_0\rangle|^2$ for $C^{+-}(\mathbf{k},\omega)$.

Figure 5 shows the intensity plot of $C^z(\mathbf{k},\omega)$ [panels (a) and (b)] and the intensity of each peak (i.e., $|\langle \tau, -\mathbf{k}_0|S^z_{-\mathbf{k}}|\phi_0\rangle|^2/N$; see panels (c)–(f)] along $(k_x,k_y) = (k,k)$. First, we have to note for CO and MI that there is no contribution from the one spin-wave excitation modes, i.e., $\langle \tau, -\mathbf{k}_0|S^z_{-\mathbf{k}}|\phi_0\rangle = 0$. For SF, two excitation bands contribute to the spin-spin correlation as seen in Figs. 5(a) and 5(c), since there is no band folding. Around $\mathbf{k} = (0,0)$, the excitations consist of a NG mode (whose intensity grows linearly with k), and a massive mode (whose intensity grows as k^4), and we also find a roton mode around (π,π). Such behaviors match those of the dynamical structure factor in the boson systems.[20,21] As can be seen in Fig. 5(f), which shows the intensity of peak against h at the zone boundary $\mathbf{Q} = (\pi,\pi)$, the intensity rapidly increases toward the SF/SS or SF/CO boundaries. This can be regarded as a hallmark for the phase transition for SS or CO.

If we turn to the SS state in Figs. 5(b), 5(d), and 5(e), there are four single-particle excitations that contribute to the spin-spin correlation. Since the Z_2 symmetry is broken in SS, the selection rule for the matrix elements appearing in Eqs. (21) and (22) is the same for (k_x,k_y) as for $(k_x + \pi, k_y + \pi)$, so that the NG mode in Fig. 5(b) appears around both (0,0)

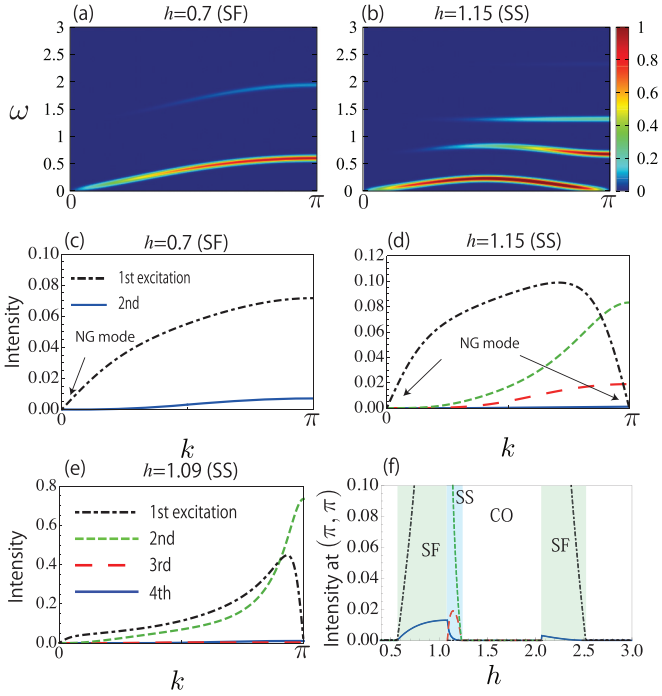

FIG. 5. (Color online) (a),(b) Color-coded intensity of $C^z(\mathbf{k},\omega)$ against $k_x = k_y = k$ for a SF phase with $h = 0.7$ (a) and for a SS phase with $h = 1.15$ (b), with $ZJ_1 = 0.84$ and $ZJ_2 = 0.68$. A Gaussian of width $\delta = 0.03J_0$ is used to smooth the δ functions in $C^z(\mathbf{k},\omega)$. (c)–(f) The intensity of peaks of $C^z(\mathbf{k},\omega)$ against $k_x = k_y = k$ for single spin-wave states for $h = 0.7$ (c), $h = 1.15$ (d), and $h = 1.09$ (e), with $ZJ_1 = 0.84$ and $ZJ_2 = 0.68$. For the homogeneous states, the first (second) band is represented by black (blue) lines. For the state with broken Z_2 symmetry, blue, red, green, and black lines represent the first, second, third, and fourth excitations, respectively. (f) The intensity against h at $(k_x,k_y) = (\pi,\pi)$. Note the difference in the scale of the vertical axis between panels (c)–(f).

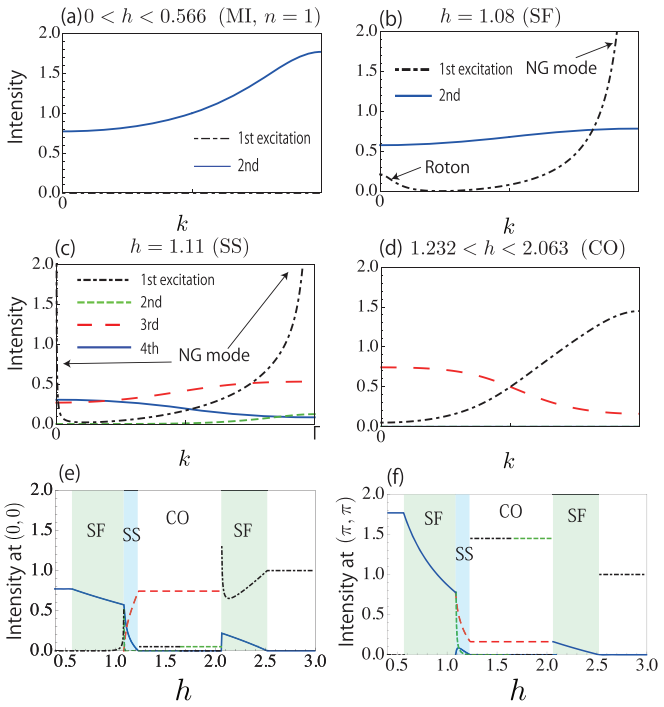

FIG. 6. (Color online) The intensity of peaks against $k_x = k_y = k$ for single spin-wave states in the $C^{+-}(\mathbf{k},\omega)$ correlation with $ZJ_1 = 0.84$ and $ZJ_2 = 0.68$. Panel (a) is for $0 < h < 0.566$ (MI, $n = 1$), (b) $h = 1.08$ (SF), (c) $h = 1.11$ (SS), and (d) $1.232 < h < 2.063$ (CO). For the homogeneous states, the first and the second bands are represented by black and blue lines, respectively. For the state with Z_2 symmetry broken, the blue, red, green, and black lines mean the first, second, third, and fourth excitations, respectively. Panel (e) shows the intensity against h at $(k_x,k_y) = (0,0)$, and (f) shows that at $(k_x,k_y) = (\pi,\pi)$.

and (π,π). It turns out that the intensity of the fourth band in the SS phase rapidly decreases toward the boundary to CO. The intensity of this band is much weaker than those for the other bands in the SS region. At long wavelengths ($k \sim 0$), the intensity also starts from 0 in most part of the SS state. Only the NG mode has an intensity increasing linearly with k, while the other three modes increase like k^4. Just after the transition to the SS state in Fig. 5(e), the dominant excitations are the lowest two modes. Away from the phase boundary in Fig. 5(d), the intensities of the lowest three modes become comparable with each other. The fact that the massive mode [the third excitation mode around (0,0) $\in \mathbf{BZ}/2$)] has a significant intensity for the C^z correlation function reflects the property of the mode that it becomes coupled with the density modulation in SS. We also find that the intensity of the NG mode vanishes at the zone boundary in SS. This reflects the fact that zero-energy excitation is only coupled with the phase oscillation of the order parameter. Another characteristic property is that the intensity is stronger around (π,π) than around (0,0) when we compare $(k_x,k_y) \in \mathbf{BZ}/2$ and $(k_x + \pi, k_y + \pi) \notin \mathbf{BZ}/2$. Therefore, the bands can be observed more clearly around (π,π), as seen in Fig. 5(b).

Finally we discuss the behavior of the correlation C^{+-}. Figure 6 shows the intensity ($|\langle\tau, -\mathbf{k_0}|\hat{M}^\dagger_{xy,-\mathbf{k}}|\phi_0\rangle|^2/N$) for C^{+-} along $(k_x,k_y) = (k,k)$. As seen in Eq. (24), single spin-wave states contribute to the matrix element in the insulating phases (MI, CO). It turns out that in MI ($n = 1$) in Fig. 6(a), only the second excitation band has a significant intensity, which does not depend on h within the present approximation. In the CO state in Fig. 6(d), we can see two bands in the spectrum, i.e., the first band (the second at higher h) and the third band [Fig. 6(d)]. Namely, as h increases in CO, the two bands change their orders; hence, the nature of the first and second bands changes. This can be seen in Figs. 6(e) and 6(f), where the intensity of the first band is finite at lower h in CO, while the intensity of the second band is finite at higher h. In MI ($n = 2$), only the first band is observed, whose intensity is $|\langle\tau, -\mathbf{k}_0|\hat{M}^\dagger_{xy,-\mathbf{k}}|\phi_0\rangle|^2/N = 1$ throughout (not shown). In the SF phase, both bands have contributions to C^{+-}. An interesting observation is that the intensity to the NG mode diverges like $1/|(k_x - \pi, k_y - \pi)|$ toward (π,π). Therefore, the NG mode is expected to be observed clearly. As for the roton mode, its intensity increases near the boundary of SF/SS or SF/CO; see Figs. 6(b) and 6(e). This increase is a precursor to the breakdown of Z_2 symmetry. In the SS phase in Fig. 6(c), the NG mode becomes intense toward $\mathbf{k} = (0,0),(\pi,\pi)$. More concretely, the intensity

of the first band diverges like $1/|(k_x,k_y)|$ at $\mathbf{k} = (0,0)$ and like $1/|(k_x - \pi, k_y - \pi)|$ at $\mathbf{k} = (\pi,\pi)$. On the other hand, it turns out that the intensities of the second to fourth bands in the SS phase strongly depend on (J_1, J_2, h). Given the correspondence between the Bose-Hubbard model and the spin system, these characteristic behaviors in SS revealed here can be expected in cold atoms in optical lattice as well.

V. CONCLUSION

In this paper we have studied the frustrated spin-dimer model with the bond operator and the generalized spin-wave theory. First we have obtained the mean-field phase diagram, which can be directly compared with that of the extended Bose-Hubbard model. We have revealed how the SS state emerges in this model, and found that there is a phase ("SF") which involves $|1,0\rangle$ state and hence has no counterpart in the Bose-Hubbard model. In addition, we point out that the enlarged SS region for large V ($\gtrsim ZU$) in the Bose-Hubbard model does not occur in the spin model, because the "SF" phase takes over instead.

Second, we have obtained the excitation modes, especially the excitation spectra around the SS regions. We have found that the dip corresponding to a roton mode completely softens at the boundary of SS, and that a NG mode has a linear dispersion even in the SS state. We have also microscopically derived within the generalized linear spin-wave theory an analytical relation between the velocity of the NG mode, order parameter and spin susceptibility, which agrees with the relation derived from hydrostatic treatments. As for the properties of the excitation modes, it turns out that, in the SF state, the massive mode does not couple with density modulations, while in the SS state there is a coupling.

Third, we have calculated the spin-spin correlations C^z and C^{+-}. C^z corresponds in the Bose system to the dynamical structure factor, while C^{+-} corresponds to the lesser Green's function. In the SF state, the behavior of C^z is similar to its counterpart for cold atoms. The resonance of the intensity of the roton mode is thought to be a precursor to the breaking of Z_2 symmetry (phase transition to CO or SS). In the SS state, the intensity of the NG (sound) mode peak vanishes at the boundary of the first Brillouin zone, while the third excitation band becomes significant, which reflects the property of the difference in the excitation between SS and SF mentioned above. As for C^{+-}, the spin-wave theory predicts that some of the bands have significant intensities in the insulating phases (MI,CO). On the other hand, the NG mode is expected to be clearly observed in the spin-spin correlation, while the intensity of the roton mode can be regard as an evidence for the phase transition to CO or SS. The properties of SS revealed here for the spin model should be applicable to the SS phase in Bose systems. Hence, the results should be important probes in searching SS in a wide range of systems.

ACKNOWLEDGMENTS

We wish to thank D. Yamamoto and T. Morimoto for helpful discussions.

APPENDIX A

Let us here display an 8×8 matrix $\hat{H}_{\rm eff}(\mathbf{k})$ explicitly, whose form is

$$\hat{H}_{\rm eff}(\mathbf{k}) = \begin{bmatrix} E_+^A & E_\pm^A & C_+ & C'_\pm & 0 & 0 & D_+ & D_\pm \\ E_\pm^A & E_-^A & C_\pm & C_- & 0 & 0 & D'_\pm & D_- \\ C_+ & C_\pm & E_+^B & E_\pm^B & D_+ & D'_\pm & 0 & 0 \\ C'_\pm & C_- & E_\pm^B & E_-^B & D_\pm & D_- & 0 & 0 \\ 0 & 0 & D_+ & D_\pm & E_+^A & E_\pm^A & C_+ & C'_\pm \\ 0 & 0 & D'_\pm & D_- & E_\pm^A & E_-^A & C_\pm & C_- \\ D_+ & D'_\pm & 0 & 0 & C_+ & C_\pm & E_+^B & E_\pm^B \\ D_\pm & D_- & 0 & 0 & C'_\pm & C_- & E_\pm^B & E_-^B \end{bmatrix}. \tag{A1}$$

Expressions for the elements are

$$\begin{aligned} E_+^\lambda &= (J_0 - h)\big(u_\lambda^2 f_\lambda^2 - v_\lambda^2 f_\lambda^2\big) + (J_0 + h)\big(u_\lambda^2 g_\lambda^2 - v_\lambda^2 g_\lambda^2\big) \\ &\quad - J_2 Z v_\lambda v_{\bar\lambda} u_\lambda u_B (f_\lambda + g_\lambda)(f_{\bar\lambda} + g_{\bar\lambda}) \\ &\quad + \left(J_1 + \frac{J_2}{2}\right) Z v_\lambda^2 u_\lambda^2 (f_\lambda^2 - g_\lambda^2)(f_{\bar\lambda}^2 - g_{\bar\lambda}^2) + E_{\rm CON}, \end{aligned} \tag{A2}$$

$$\begin{aligned} E_-^\lambda &= (J_0 - h)\big(g_\lambda^2 - v_\lambda^2 f_\lambda^2\big) + (J_0 + h)\big(f_\lambda^2 - v_\lambda^2 g_\lambda^2\big) \\ &\quad - \left(J_1 + \frac{J_2}{2}\right) Z v_{\bar\lambda}^2 \big(f_\lambda^2 - g_\lambda^2\big)\big(f_{\bar\lambda}^2 - g_{\bar\lambda}^2\big) + E_{\rm CON}, \end{aligned} \tag{A3}$$

$$\begin{aligned} E_\pm^\lambda &= 2h g_\lambda u_\lambda f_\lambda - 2\left(J_1 + \frac{J_2}{2}\right) Z v_{\bar\lambda}^2 u_\lambda f_\lambda g_\lambda \big(f_{\bar\lambda}^2 - g_{\bar\lambda}^2\big) \\ &\quad + \frac{J_2}{2} Z v_{\bar\lambda} v_\lambda u_{\bar\lambda} (f_{\bar\lambda} g_\lambda - g_{\bar\lambda} f_\lambda - f_\lambda f_{\bar\lambda} + g_\lambda g_{\bar\lambda}), \end{aligned} \tag{A4}$$

$$\begin{aligned} C_+ &= 2\gamma(\mathbf{k})\Bigg[\frac{J_2}{2}\big(v_A^2 v_B^2 + u_A^2 u_B^2\big)(f_A f_B + g_A g_B) \\ &\quad - \frac{J_2}{2}\big(v_A^2 u_B^2 + v_B^2 u_A^2\big)(f_A g_B + f_B g_A) \\ &\quad + \left(J_1 + \frac{J_2}{2}\right) v_A v_B u_A u_B \big(f_A^2 - g_A^2\big)\big(f_B^2 - g_B^2\big)\Bigg], \end{aligned} \tag{A5}$$

$$\begin{aligned} C_- &= \gamma(\mathbf{k}) J_2 u_A u_B (g_A g_B + f_A f_B) \\ &\quad + 8\gamma(\mathbf{k})\left(J_1 + \frac{J_2}{2}\right) g_A g_B f_A f_B v_A v_B, \end{aligned} \tag{A6}$$

$$\begin{aligned} C_\pm &= \gamma(\mathbf{k}) J_2 \big[u_A u_B^2 (f_A g_B - f_B g_A) + v_B^2 u_A (g_A g_B - f_A f_B)\big] \\ &\quad - 4\gamma(\mathbf{k})\left(J_1 + \frac{J_2}{2}\right) v_A v_B u_B g_A f_A \big(f_B^2 - g_B^2\big), \end{aligned} \tag{A7}$$

$$\begin{aligned} C'_\pm &= \gamma(\mathbf{k}) J_2 \big[u_B u_A^2 (f_B g_A - f_A g_B) + v_A^2 u_B (g_A g_B - f_A f_B)\big] \\ &\quad - 4\gamma(\mathbf{k})\left(J_1 + \frac{J_2}{2}\right) v_B v_A u_A g_B f_B \big(f_A^2 - g_A^2\big), \end{aligned} \tag{A8}$$

$$\begin{aligned} D_+ &= 2\gamma(\mathbf{k})\Bigg[-\frac{J_2}{2}\big(v_A^2 u_B^2 + v_B^2 u_A^2\big)(f_A f_B + g_A g_B) \\ &\quad + \frac{J_2}{2}\big(v_A^2 v_B^2 + u_A^2 u_B^2\big)(g_B f_A + g_A f_B) \\ &\quad + \left(J_1 + \frac{J_2}{2}\right) v_A v_B u_A u_B \big(f_A^2 - g_A^2\big)\big(f_B^2 - g_B^2\big)\Bigg], \end{aligned} \tag{A9}$$

$$D_- = -\gamma(\mathbf{k})J_2 u_A u_B (g_A f_B + g_B f_A) + 8\gamma(\mathbf{k})\left(J_1 + \frac{J_2}{2}\right) v_A v_B g_A g_B f_A f_B, \quad \text{(A10)}$$

$$D_\pm = \gamma(\mathbf{k})J_2\left[v_A^2 u_B (f_A g_B - g_A f_B) + u_B u_A^2 (f_A f_B - g_A g_B)\right] - 4\gamma(\mathbf{k})\left(J_1 + \frac{J_2}{2}\right) v_B v_A u_A g_B f_B \left(f_A^2 - g_A^2\right), \quad \text{(A11)}$$

and

$$D'_\pm = \gamma(\mathbf{k})J_2\left[v_B^2 u_A (f_B g_A - g_B f_A) + u_A u_B^2 (f_A f_B - g_A g_B)\right] - 4\gamma(\mathbf{k})\left(J_1 + \frac{J_2}{2}\right) v_A v_B u_B g_A f_A \left(f_B^2 - g_B^2\right). \quad \text{(A12)}$$

Here Z is the coordination number, $\gamma(\mathbf{k}) = \sum_{a=1}^{d} \cos(k_a)$, $\lambda = A, B$, and $\bar{\lambda}$ denotes the sublattices other than λ. E_{CON} in Eqs. (A2) and (A3) is

$$E_{\mathrm{CON}} = -ZJ_2 u_A u_B v_A v_B (f_A + g_A)(f_B + g_B) - Z\left(J_1 + \frac{J_2}{2}\right) v_A v_A v_B v_B \left(f_A^2 - g_A^2\right)\left(f_B^2 - g_B^2\right). \quad \text{(A13)}$$

APPENDIX B: DERIVATION OF EQ. (19)

We show how we can derive an analytic expression, Eq. (19). The idea is that, if we are only interested in the velocity, we can make use of the equations governing the coefficients for bosons $(t^\dagger, s^\dagger)$ in the ground state. A similar idea is used in the context of Gutzwiller approximation for boson models.[21] The proof consists of three steps. In the first step, we introduce another way to derive the excitation. In the second step, we show that the resultant excitation spectrum is the same as that in the main text. In the third step, we prove Eq. (19) within the approach introduced in the first step. We start from Eq. (7), which neglects the existence of $|1,0\rangle$, and uses the language of Bose systems [Eq. (9)] to characterize parameters in the Hamiltonian. Note that, in the following, we also change $s^\dagger \to t_0^\dagger$ and $y \to x_0$ to simplify the notation.

1. First step

The original assumption is that the form of the ground state is $\prod_{i\in A}(x_{A,1}t_{i+}^\dagger + x_{A,0}t_{i0}^\dagger + x_{A,-1}t_{i-}^\dagger)\prod_{i\in B}(x_{B,1}t_{i+}^\dagger + x_{B,0}t_{i0}^\dagger + x_{B,-1}t_{i-}^\dagger)|\mathrm{vac}\rangle$, whose norm is 1. We extend this to assume that the dynamics is confined to this type of states and that when we consider the dynamics of site g the effect of the surrounding state can be regarded as a mean field (which is an idea similar to the Gutzwiller approach for the Bose-Hubbard model[21]). In other words, to consider the dynamics of the state on site g at time τ, we use the local Hamiltonian,

$$H_g(\tau) = -t\sum_{i_g}\left[(t_{g+}^\dagger t_{g0} + t_{g0}^\dagger t_{g-})\phi_{i_g}(\tau) + \mathrm{H.c.}\right] + V\sum_{i_g}(t_{g+}^\dagger t_{g+} - t_{g-}^\dagger t_{g-})\delta n_{i_g}(\tau) + \frac{U}{2}(t_{g+}^\dagger t_{g+} + t_{g-}^\dagger t_{g-}) - h(t_{g+}^\dagger t_{g+} - t_{g-}^\dagger t_{g-}), \quad \text{(B1)}$$

where i_g stands for the nearest neighbors of g, $\phi_i(\tau) = \langle t_{i0}^\dagger t_{i+} + t_{i-}^\dagger t_{i0}\rangle = x_{i,0}^*(\tau)x_{i,1}(\tau) + x_{i,-1}^*(\tau)x_{i,0}(\tau)$ and $\delta n_i(\tau) = \langle t_{i+}^\dagger t_{i+} - t_{i-}^\dagger t_{i-}\rangle = x_{i,1}^*(\tau)x_{i,1}(\tau) - x_{i,-1}^*(\tau)x_{i,-1}(\tau)$. Then the equation of motion for the coefficient is

$$i\frac{dx_{g,\theta}(\tau)}{d\tau} = -t\sum_{\sigma,\theta'}[\phi_{g+\sigma}\delta_{\theta,\theta'+1} + \phi_{g+\sigma}^*\delta_{\theta,\theta'-1}]x_{g,\theta'}(\tau) + \left[\frac{U}{2}\theta^2 - \theta h + \theta V\left(\sum_\sigma \delta n_{g+\sigma}\right)\right]x_{g,\theta}(\tau), \quad \text{(B2)}$$

where $\theta = \pm 1, 0$. In the ground state, the local Hamiltonian can be different between A, B sublattices, which we express as H_A, H_B. We can express the variational ground state as $\prod_i(\sum_\theta d_{i,\theta}^{0\lambda}t_{i,\theta}^\dagger)|\mathrm{vac}\rangle (i \in \lambda)$, where $d_{i,\theta}^{0\lambda}$ is the optimized parameter. Then the state on sublattice λ $(\sum_\theta d_\theta^{0\lambda}t_\theta^\dagger)|\mathrm{vac}\rangle)$ is an eigenstate of H_λ with an eigenvalue ω_λ. We derive the excitation spectrum by considering the stationary solutions around the ground state. In order to do this, we consider $x_{g,\theta}^\lambda(\tau) = [d_{g,\theta}^{0\lambda} + d_{g,\theta}'^{\lambda}(\tau)]\exp(-i\omega_\lambda\tau)$, where we have defined $d_{g,\theta}'^{\lambda}(\tau)$, which is assumed to be small. The equation of motion is linearized with respect to $d_{g,\theta}'^{\lambda}(\tau)$, where we consider the stationary solutions with a form

$$d_{\mathbf{l},\theta}'^{\lambda}(\tau) = u_{\mathbf{k}\theta}^\lambda \exp[i(\mathbf{k}\cdot\mathbf{l} - \omega_\mathbf{k}\tau)] + v_{\mathbf{k}\theta}^{\lambda *}\exp[-i(\mathbf{k}\cdot\mathbf{l} - \omega_\mathbf{k}\tau)]. \quad \text{(B3)}$$

The resultant equation is

$$\omega_\mathbf{k}\begin{bmatrix}\boldsymbol{u}^A\\ \boldsymbol{u}^B\\ \boldsymbol{v}^A\\ \boldsymbol{v}^B\end{bmatrix} = \begin{bmatrix} W_{A,A} & W_{A,B} & 0 & V_{A,B}\\ W_{B,A} & W_{B,B} & V_{B,A} & 0\\ 0 & -V_{A,B} & -W_{A,A} & -W_{A,B}\\ -V_{B,A} & 0 & -W_{B,A} & -W_{B,B}\end{bmatrix}\begin{bmatrix}\boldsymbol{u}^A\\ \boldsymbol{u}^B\\ \boldsymbol{v}^A\\ \boldsymbol{v}^B\end{bmatrix}. \quad \text{(B4)}$$

Here $\mathrm{W}_{\lambda,\lambda'}, \mathrm{V}_{\lambda,\lambda'}$ are 3×3 matrices with $\boldsymbol{u}^\lambda = (u_{\mathbf{k},1}^\lambda, u_{\mathbf{k},0}^\lambda, u_{\mathbf{k},-1}^\lambda)^T$ and $\boldsymbol{v}^\lambda = (v_{\mathbf{k},1}^\lambda, v_{\mathbf{k},0}^\lambda, v_{\mathbf{k},-1}^\lambda)^T$. In the following let us denote the 12×12 matrix as $\Upsilon(\mathbf{k})$. The elements of this matrix are

$$\begin{aligned} W_{\lambda,\lambda,\theta,\theta'} &= \left(\frac{U}{2}\theta^2 - h\theta - \omega_\lambda + \theta V Z\delta n_\lambda^0\right)\delta_{\theta,\theta'} - Zt\phi_{\bar{\lambda}}^0(\delta_{\theta,\theta'+1} + \delta_{\theta,\theta'-1}),\\ W_{\lambda,\bar{\lambda},\theta,\theta'}(\mathbf{k}) &= -t\gamma(\mathbf{k})\left(d_{\theta-1}^{0\lambda}d_{\theta'-1}^{0\bar{\lambda}} + d_{\theta+1}^{0\lambda}d_{\theta'+1}^{0\bar{\lambda}}\right) + V\theta\theta'\gamma(\mathbf{k})d_\theta^{0\lambda}d_{\theta'}^{0\bar{\lambda}},\\ V_{\lambda,\bar{\lambda},\theta,\theta'}(\mathbf{k}) &= -t\gamma(\mathbf{k})\left(d_{\theta-1}^{0\lambda}d_{\theta'+1}^{0\bar{\lambda}} + d_{\theta+1}^{0\lambda}d_{\theta'-1}^{0\bar{\lambda}}\right) + V\theta\theta'\gamma(\mathbf{k})d_\theta^{0\lambda}d_{\theta'}^{0\bar{\lambda}}, \end{aligned} \quad \text{(B5)}$$

where δn_λ^0 and ϕ_λ^0 denote, respectively, δn and ϕ on sublattice λ in the ground state. Note that, to derive Eqs. (B2) and (B4), $\sum_\theta |x_\theta|^2 = 1$ is assumed. Therefore, the solutions of Eq. (B4) which satisfy $\sum_\theta |x_\theta|^2 = 1$ are physical. This is why the 12×12 matrix in Eq. (B4) and the 8×8 matrix, $\hat{H}_{\mathrm{eff}}(\mathbf{k})$, give the same results.

2. Second step

The idea for deriving above equation of motion does not depend on the choice of the basis employed. Let us define another local Hamiltonian for site g

$$\begin{aligned} H'_g = &-t\sum_{i_g}\left[(t^\dagger_{g+}t_{g0}+t^\dagger_{g0}t_{g-})\left(t^\dagger_{i_g0}t_{i_g+}+t^\dagger_{i_g-}t_{i_g0}\right)+\text{H.c.}\right] \\ &+V\sum_{i_g}(t^\dagger_{g+}t_{g+}-t^\dagger_{g-}t_{g-})\left(t^\dagger_{i_g+}t_{i_g+}-t^\dagger_{i_g-}t_{i_g-}\right) \\ &+\frac{U}{2}(t^\dagger_{g+}t_{g+}+t^\dagger_{g-}t_{g-})-h(t^\dagger_{g+}t_{g+}-t^\dagger_{g-}t_{g-}), \end{aligned} \tag{B6}$$

where we have picked up the part of the Hamiltonian Eq. (7) that involves site g. Then let $\{b'^\dagger_{i,\theta}\}$ be a set of bosonic creation operators transformed from $\{t^\dagger_{i,\theta}\}$, i.e., $b'^\dagger_{i,\theta}=\sum_{\theta'}U^{(i)}_{\theta,\theta'}t^\dagger_{i,\theta'}$ with $U^{(i)}$ an arbitrary site-dependent unitary matrix, and express a state as $|\psi(\tau)\rangle=\prod_i(\sum_\theta\chi_{i,\theta}(\tau)b'^\dagger_{i,\theta})|\text{vac}\rangle$, where $\chi_{i,\theta}$ is a complex coefficient. As far as $|\psi(\tau)\rangle$ is normalized the equation of motion introduced in the first step is expressed as

$$\begin{aligned} i\frac{d}{dt\tau}\chi_{g,\theta}(\tau) = &\langle\text{vac}|b'_{g,\theta}\prod_{i\neq g}\left[\sum_{\theta'}\chi^*_{i,\theta'}(t)b'_{i,\theta'}\right]H'_g \\ &\times\prod_i\left[\sum_\theta\chi_{i,\theta'}(t)b'^\dagger_{i,\theta'}\right]|\text{vac}\rangle, \end{aligned} \tag{B7}$$

with $b'^\dagger=t^\dagger$. However, the evolution of the state with Eq. (B7) does not depend on the choice of $\{b'^\dagger_{i,\theta}\}$. As is explained in the following, it turns out that, if we take $b'^\dagger=b^\dagger$, the equation for the stationary solution around the ground state leads to the same form as the equation for the excitation spectrum within the spin-wave theory; see Eq (14). Therefore, the excitation spectrum derived from the method in the first step is same as that from the spin-wave theory in the main part of this article. Let us take $b'^\dagger$ equal to $b^\dagger$ defined in Eq. (12). In this case $\prod_i b^\dagger_{0,i}|\text{vac}\rangle$ is the variational ground state, $|\text{GS}\rangle$. Let

$$\begin{aligned} &\chi_{i,\theta}(t)=C_{i,\theta}(t)\exp(-i\omega_\lambda t), \\ &C_{i,\theta}(t)=\begin{cases}1+c'_{i,0}, & \theta=0,\\ c'_{i,\theta} & \theta\neq 0,\end{cases} \end{aligned} \tag{B8}$$

where $i\in\lambda$. Linearizing the equation, we obtain

$$\begin{aligned} i\frac{d}{d\tau}c'_{g,\theta}(\tau) = &\sum_{\theta'\neq 0}\alpha^\lambda_{\theta,\theta'}c'_{g,\theta'}(\tau) \\ &+\sum_{i\neq g,\theta'\neq 0}\left[\beta^\lambda_{\theta,\theta'}c'_{i,\theta'}(\tau)+\gamma^\lambda_{\theta,\theta'}c'^*_{i,\theta'}(\tau)\right], \end{aligned} \tag{B9}$$

where

$$\begin{aligned} \alpha^\lambda_{\theta,\theta'} &= \langle\text{GS}|b^\dagger_{g,0}b_{g,\theta}(H'_g-\omega_\lambda)b^\dagger_{g,\theta'}b_{g,0}|\text{GS}\rangle, \\ \beta^\lambda_{\theta,\theta'} &= \langle\text{GS}|b^\dagger_{g,0}b_{g,\theta}(H'_g-\omega_\lambda)b^\dagger_{i,\theta'}b_{i,0}|\text{GS}\rangle, \\ \gamma^\lambda_{\theta,\theta'} &= \langle\text{GS}|b^\dagger_{g,0}b_{g,\theta}b^\dagger_{i,0}b_{i,\theta'}(H'_g-\omega_\lambda)|\text{GS}\rangle, \end{aligned} \tag{B10}$$

with $g\in\lambda$. Strictly speaking, the form of this equation is a bit different from the equation of motion obtained by linearizing Eq. (B2), but it turns out that Eq. (B9) and the equation linearized from Eq. (B2) give the same solutions as far as both of the solutions satisfy the normalization condition $\sum_\theta|x_\theta|^2=\sum_\theta|\chi_\theta|^2=1$; i.e., $\boldsymbol{d^0}\cdot\boldsymbol{d'}$ is purely imaginary, where $\boldsymbol{d^0},\boldsymbol{d'}$ are defined below Eq. (B2).

When we look at Eq. (B9), we notice that the evolution of the coefficients does not depend on the $\theta=0$ component. Therefore, when we consider the stationary solution around the ground state, we only have to deal with an eigenvalue problem for the $\theta=\pm$ components, and then we can decide the evolution of the $\theta=0$ component. As in the first step, we try to find the solution with the form

$$c'^\lambda_{i,\theta}=u'^\lambda_\theta\exp(i\mathbf{k}\cdot\mathbf{r}_i-i\omega_\mathbf{k}t)+v'^{\lambda*}_\theta\exp(-i\mathbf{k}\cdot\mathbf{r}_i+i\omega_\mathbf{k}t). \tag{B11}$$

Then the eigenvalue problem for the $\theta=\pm$ components reads

$$\begin{aligned} \omega_\mathbf{k}\begin{bmatrix}\boldsymbol{u'}^A\\ \boldsymbol{u'}^B\\ \boldsymbol{v'}^A\\ \boldsymbol{v'}^B\end{bmatrix} = &\begin{bmatrix}W'_{A,A} & W'_{A,B} & 0 & V'_{A,B}\\ W'_{B,A} & W'_{B,B} & V'_{B,A} & 0\\ 0 & -V'_{A,B} & -W'_{A,A} & -W'_{A,B}\\ -V'_{B,A} & 0 & -W'_{B,A} & -W'_{B,B}\end{bmatrix} \\ &\times\begin{bmatrix}\boldsymbol{u'}^A\\ \boldsymbol{u'}^B\\ \boldsymbol{v'}^A\\ \boldsymbol{v'}^B\end{bmatrix}, \end{aligned} \tag{B12}$$

where W' and V' are 2×2, $\boldsymbol{u'}^\lambda=(u'^\lambda_{\mathbf{k},1},u'^\lambda_{\mathbf{k},-1})^T$, $\boldsymbol{v'}^\lambda=(v'^\lambda_{\mathbf{k},1},v'^\lambda_{\mathbf{k},-1})^T$, and

$$\begin{aligned} &W_{\lambda,\lambda,\theta,\theta'}=\alpha^\lambda_{\theta,\theta'},\quad W_{\lambda,\bar\lambda,\theta,\theta'}(\mathbf{k})=\gamma(\mathbf{k})\beta^\lambda_{\theta,\theta'}, \\ &V_{\lambda,\bar\lambda,\theta,\theta'}(\mathbf{k})=\gamma(\mathbf{k})\gamma^\lambda_{\theta,\theta'}. \end{aligned} \tag{B13}$$

By directly evaluating α, β, and γ, one can see that the matrix in Eq. (B12) is nothing but $\sum\hat H_{\text{eff}}(\mathbf{k})$. Therefore, the method introduced in the first step gives the same excitation spectrum as in the spin-wave theory introduced in the main part of this paper.

3. Third step

We can then move on to show the relationship between the velocity of the NG mode, the order parameters, and the spin susceptibility in the way introduced in the first step. First, one can derive an important identity,

$$\begin{aligned} &\left(\frac{U}{2}\theta^2-h\theta-\omega_\lambda+\theta VZ\delta n^{0\bar\lambda}\right)d^{0\lambda}_\theta \\ &\quad -Zt\phi^{0\bar\lambda}\sum_{\theta'}(\delta_{\theta,\theta'+1}+\delta_{\theta,\theta'-1})d^{0\lambda}_{\theta'}=0, \end{aligned} \tag{B14}$$

from the fact that $x^\lambda_\theta(t)=d^{0\lambda}_\theta\exp(-i\omega_\lambda)$ is a stationary solution of Eq. (B2). Then the first derivative of this equation with respect to h is

$$\begin{aligned} \left(\theta+\frac{\partial\omega_\lambda}{\partial h}\right)d^{0\lambda}_\theta = &\sum_{\theta'}W_{\lambda,\lambda,\theta,\theta'}\frac{\partial d^{0\lambda}_{\theta'}}{\partial h} \\ &+\sum_{\theta'}[W_{\lambda,\bar\lambda,\theta,\theta'}(\mathbf{0})+V_{\lambda,\bar\lambda,\theta,\theta'}(\mathbf{0})]\frac{\partial d^{0\bar\lambda}_{\theta'}}{\partial h}. \end{aligned} \tag{B15}$$

This is the key equation. We can readily find three solutions of Eq. (B4) at $\mathbf{k} = \mathbf{0}$ as

$$\begin{aligned} &u^{\lambda}_{\mathbf{0},\theta} \equiv \theta d^{0\lambda}_{\theta}, \quad \boldsymbol{v}^{\lambda}_{\mathbf{0}} = -\boldsymbol{u}^{\lambda}_{\mathbf{0}}, \quad \omega_{\mathbf{0}} = 0, \\ &u^{A}_{\mathbf{0},\theta} \equiv d^{0A}_{\theta}, \quad u^{B}_{\mathbf{0},\theta} = 0, \quad \boldsymbol{v}^{\lambda}_{\mathbf{0}} = -\boldsymbol{u}^{\lambda}_{\mathbf{0}}, \quad \omega_{\mathbf{0}} = 0, \\ &u^{B}_{\mathbf{0},\theta} \equiv d^{0B}_{\theta}, \quad u^{A}_{\mathbf{0},\theta} = 0, \quad \boldsymbol{v}^{\lambda}_{\mathbf{0}} = -\boldsymbol{u}^{\lambda}_{\mathbf{0}}, \quad \omega_{\mathbf{0}} = 0. \end{aligned} \tag{B16}$$

The first one is independent of the other two as far as the U(1) symmetry is broken. What we do next is to expand the equation around $\mathbf{k} \approx \mathbf{0}$ to find the lowest-energy solution. In order to do this, we expand as

$$\begin{aligned} u^{\lambda}_{\mathbf{k},\theta} &= u^{(0)\lambda}_{\theta} + u^{(1)\lambda}_{\mathbf{k},\theta} + u^{(2)\lambda}_{\mathbf{k},\theta} + \cdots, \\ v^{\lambda}_{\mathbf{k},\theta} &= v^{(0)\lambda}_{\theta} + v^{(1)\lambda}_{\mathbf{k},\theta} + v^{(2)\lambda}_{\mathbf{k},\theta} \cdots, \\ \omega_{\mathbf{k}} &= \omega^{(0)} + \omega^{(1)}_{\mathbf{k}} + \omega^{(2)}_{\mathbf{k}} \cdots, \end{aligned} \tag{B17}$$

and

$$\Upsilon(\mathbf{k}) = \Upsilon_0 + \Upsilon^{(2)}(\mathbf{k}) + \cdots. \tag{B18}$$

In the expansion for $\Upsilon(\mathbf{k})$, there is no first-order component of k [$\Upsilon^{(1)}(\mathbf{k})$], because the $\mathbf{k}$ dependence arises through $\gamma(\mathbf{k})$. We start with

$$u^{\lambda}_{\mathbf{0},\theta} \equiv \left(\theta + \frac{\partial \omega_{\lambda}}{\partial h}\right) d^{0\lambda}_{\theta}, \quad v^{\lambda}_{\mathbf{0}} = -u^{\lambda}_{\mathbf{0}}, \quad \omega_{\mathbf{0}} = 0. \tag{B19}$$

The first-order equation is

$$\omega^{(1)}_{\mathbf{k}} \begin{bmatrix} \boldsymbol{u}^{(0)} \\ \boldsymbol{v}^{(0)} \end{bmatrix} = \Upsilon_0 \begin{bmatrix} \boldsymbol{u}^{(1)} \\ \boldsymbol{v}^{(1)} \end{bmatrix}, \tag{B20}$$

where $\boldsymbol{u}^{(0)} = [(\boldsymbol{u}^{(0)A})^T, (\boldsymbol{u}^{(0)B})^T]^T$ and $\boldsymbol{v}^{(0)} = [(\boldsymbol{v}^{(0)A})^T, (\boldsymbol{v}^{(0)B})^T]^T$. With the identity Eq. (B15), the first-order solution is

$$u^{(1)\lambda}_{\mathbf{k},\theta} \equiv \omega^{(1)}_{\mathbf{k}} \frac{\partial d^{0\lambda}_{\theta}}{\partial h}, \quad \boldsymbol{v}^{\lambda}_{\mathbf{0}} = \boldsymbol{u}^{\lambda}_{\mathbf{0}}. \tag{B21}$$

We note here that $(\partial d^{0A}_1/\partial h, \partial d^{0A}_0/\partial h, \partial d^{0A}_{-1}/\partial h, \partial d^{0B}_1/\partial h, \partial d^{0B}_0/\partial h, \partial d^{0B}_{-1}/\partial h)$ is perpendicular to $(d^{0A}_1, d^{0A}_0, d^{0A}_{-1}, 0, 0, 0)$ and $(0, 0, 0, d^{0B}_1, d^{0B}_0, d^{0B}_{-1})$. These relations [Eqs. (B19)–(B21) and the orthogonality] justify starting from Eq. (B19).

The second-order equation is

$$\omega^{(1)}_{\mathbf{k}} \begin{bmatrix} \boldsymbol{u}^{(1)} \\ \boldsymbol{v}^{(1)} \end{bmatrix} + \omega^{(2)}_{\mathbf{k}} \begin{bmatrix} \boldsymbol{u}^{(0)} \\ \boldsymbol{v}^{(0)} \end{bmatrix} = \Upsilon_0 \begin{bmatrix} \boldsymbol{u}^{(2)} \\ \boldsymbol{v}^{(2)} \end{bmatrix} + \Upsilon^{(2)}(\mathbf{k}) \begin{bmatrix} \boldsymbol{u}^{(0)} \\ \boldsymbol{v}^{(0)} \end{bmatrix}. \tag{B22}$$

If we multiply $[(\boldsymbol{u}^{(0)})^T, -(\boldsymbol{v}^{(0)})^T]$ and make use of some property of W, V, then we obtain

$$\begin{aligned} \left(\omega^{(1)}_{\mathbf{k}}\right)^2 \left[\frac{\partial \delta n_A}{\partial h} + \frac{\partial \delta n_B}{\partial h}\right] &= 4k^2 t \phi_A \phi_B \\ \Longrightarrow \omega^{(1)}_{\mathbf{k}} &= \left(\frac{2t}{\kappa} \phi_A \phi_B\right)^{1/2} k. \end{aligned} \tag{B23}$$

Here $\kappa = (\frac{\partial \delta n_A}{\partial h} + \frac{\partial \delta n_B}{\partial h})/2$ is the spin susceptibility, which corresponds to the compressibility in Bose language.

[1] E. Kim and M. H. W. Chan, Nature (London) **427**, 225 (2004).
[2] D. Y. Kim and M. H. W. Chan, Phys. Rev. Lett **109**, 155301 (2012).
[3] D. L. Kovrizhin, G. V. Pai, and S. Sinha, Europhys. Lett. **72**, 162 (2005).
[4] T. Ohgoe, T. Suzuki, and N. Kawashima, Phys. Rev. Lett. **108**, 185302 (2012).
[5] V. W. Scarola and S. Das Sarma, Phys. Rev. Lett. **95**, 033003 (2005).
[6] B. Capogrosso-Sansone, C. Trefzger, M. Lewenstein, P. Zoller, and G. Pupillo, Phys. Rev. Lett. **104**, 125301 (2010).
[7] D. Yamamoto, I. Danshita, and C. A. R. Sá de Melo, Phys. Rev. A **85**, 021601(R) (2012).
[8] T. Giamarchi, C. Rugg, and O. Tcherenyshyov, Nat. Phys. **4**, 198 (2008).
[9] T. Nikuni, M. Oshikawa, A. Oosawa, and H. Tanaka, Phys. Rev. Lett. **84**, 5868 (2000).
[10] G. Misguich and M. Oshikawa, J. Phys. Soc. Jpn. **73**, 3429 (2004).
[11] K. K. Ng and T. K. Lee, Phys. Rev. Lett. **97**, 127204 (2006).
[12] P. Sengupta and C. D. Batista, Phys. Rev. Lett. **98**, 227201 (2007).
[13] N. Laflorencie and F. Mila, Phys. Rev. Lett. **99**, 027202 (2007).
[14] K. P. Schmidt, J. Dorier, A. M. Lauchli, and F. Mila, Phys. Rev. Lett. **100**, 090401 (2008).
[15] J.-D. Picon, A. F. Albuquerque, K. P. Schmidt, N. Laflorencie, M. Troyer, and F. Mila, Phys. Rev. B **78**, 184418 (2008).
[16] P. Chen, C. Y. Lai, and M. F. Yang, Phys. Rev. B **81**, 020409(R) (2010).
[17] A. F. Albuquerque, N. Laflorencie, J. D. Picon, and F. Mila, Phys. Rev. B **83**, 174421 (2011).
[18] D. Yamamoto and I. Danshita, Phys. Rev. B **88**, 014419 (2013).
[19] Y. C. Cheng, Phys. Rev. B **23**, 157 (1981).
[20] S. D. Huber, E. Altman, H. P. Büchler, and G. Blatter, Phys. Rev. B **75**, 085106 (2007).
[21] K. V. Krutitsky and P. Navez, Phys. Rev. A **84**, 033602 (2011).
[22] T. Sommer, M. Vojta, and K. W. Becker, Eur. Phys. J. B **23**, 329 (2001).
[23] K. K. Ng and T. K. Lee, Phys. Rev. B **73**, 014433 (2006).
[24] M. Matsumoto, B. Normand, T. M. Rice, and M. Sigrist, Phys. Rev. B **69**, 054423 (2004).
[25] M. Iskin, Phys. Rev. A **83**, 051606(R) (2011).
[26] Z. Zhang, K. Wierschem, I. Yap, Y. Kato, C. D. Batista, and P. Sengupta, Phys. Rev. B **87**, 174405 (2013).
[27] C. J. Hamer, O. Rojas, and J. Oitmaa, Phys. Rev. B **81**, 214424 (2010).
[28] H. Watanabe and H. Murayama, Phys. Rev. Lett. **108**, 251602 (2012).
[29] Y. Hidaka, Phys. Rev. Lett. **110**, 091601 (2013).
[30] R. T. Scalettar, G. G. Batrouni, A. P. Kampf, and G. T. Zimanyi, Phys. Rev. B **51**, 8467 (1995).
[31] I. Danshita and D. Yamamoto, Phys. Rev. A **82**, 013645 (2010).
[32] B. I. Halperin and P. C. Hohenberg, Phys. Rev. **188**, 898 (1969).
[33] M. P. A. Fisher, P. B. Weichman, G. Grinstein, and D. S. Fisher, Phys. Rev. B **40**, 546 (1989).
[34] J. Ye, Europhys. Lett. **82**, 16001 (2008).